Using machine learning to aid in the parameter optimisation process for metal-based additive manufacturing

Cassidy Silbernagel, Adedeji Aremu and Ian Ashcroft

Original citation & hyperlink:
Silbernagel, Cassidy, Adedeji Aremu, and Ian Ashcroft. "Using machine learning to aid in the parameter optimisation process for metal-based additive manufacturing." *Rapid Prototyping Journal,* Vol 26, Issue 4, pp. 625-637 (2019).

https://dx.doi.org/**10.1108/RPJ-08-2019-0213**

DOI **10.1108/RPJ-08-2019-0213**
ISSN 1355-2546

Publisher: Emerald

Using Machine Learning to aid in the parameter optimisation process for metal-based Additive Manufacturing

Abstract

Metal-based additive manufacturing is a relatively new technology used to fabricate metal objects within an entirely digital workflow. However, only a small number of different metals are proven for this process. This is partly due to the need to find a new set of parameters which can be used to successfully build an object for every new alloy investigated. There are dozens of variables which contribute to a successful set of parameters and process parameter optimisation is currently a manual process which relies on human judgement.

Here, we demonstrate the application of Machine Learning as an alternative method to determine this set of process parameters, the subject of this test is the processing of pure copper in a laser powder bed fusion printer. Data in the form of optical images were collected over the course of traditional parameter optimisation. These images were segmented and fed into a convolutional autoencoder and then clustered in order to find the clusters which best represented a high-quality result. The clusters were manually scored according to their quality and the results applied to the original set of parameters.

It was found that the machine-learned clustering and subsequent scoring reflected many of the observations which were found in the traditional parameter optimisation process.

This exercise, as well as demonstrating the effectiveness of the ML approach, indicates an opportunity to fully automate the approach to process optimisation by applying labels to the data, hence, an approach that could also potentially be suited for on-the-fly process optimisation.

Highlights

- Machine learning can aid in parameter optimisation for additive manufacturing
- Outcomes from machine learning mainly mirrored traditional parameter optimisation results
- Additional data could create an automated approach to parameter optimisation

Keywords

- laser powder bed fusion; machine learning; additive manufacturing; 3D printing; artificial intelligence; parameter optimisation;

Graphical abstract

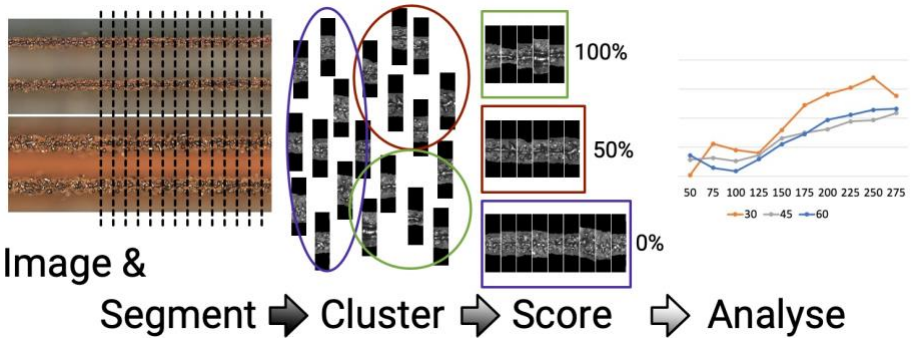

Introduction

Additive manufacturing (AM) has been called many different names over the past 30 years. Initially, AM developed from Rapid Prototyping (RP) [1] and Rapid Tooling [2] methods to a technique applicable to end-use parts, at which it became also known as Rapid Manufacturing (RM) [1], Solid Freeform Fabrication (SFF) [3] and 3D Printing (3DP) [4]. The power of AM is that it enables the design of parts that could not be easily made using traditional subtractive (e.g. CNC machines) or formative (e.g. metal casting) techniques. Within AM, Powder Bed Fusion (PBF) has been defined as "An additive manufacturing process in which thermal energy selectively fuses regions of a powder bed [5]." There are many processes that are contained within PBF including Selective Laser Melting (SLM) along with a number of other trade specific names describing the same process. Laser powder bed fusion (LPBF) is also a term for this metal-based AM process and is the preferred term used in the rest of this work.

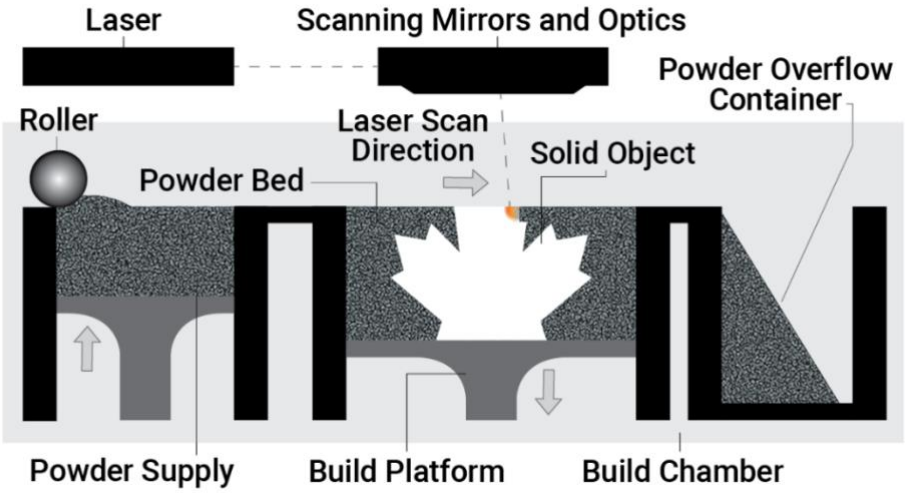

Figure 1: Laser powder bed fusion set up [6].

LPBF methods start by spreading a thin layer of powder over a build platform, as illustrated in Figure 1. This layer of powder is then selectively irradiated by a laser beam with sufficient energy to melt and fuse powder particles within the selected process zone, as well as any previously solidified layers to a depth sufficient to ensure fusing between layers. The build platform is then lowered to allow a roller to deposit the next layer of powder. The entire process is repeated, layer by layer, until a solid object is completely built. It is a common practice to heat the build platform or the build chamber to minimize thermal stresses thereby improving the quality of the object being built. The full melting of the powder enables denser parts than generally achievable by sintering alone. LPBF has now matured from a research tool to industrial application and is being used in health care [7,8], automotive [9], and aerospace [10] applications. However, propagation of LPBF across these and other industries has been greatly constrained by limited diversity in base materials.

Additive manufacturing is often touted as a purely digital manufacturing method; however, it currently requires considerable manual intervention and decision making at all stages of the process. This particularly occurs when new materials are introduced and appropriate processing parameters for high density parts with minimal defects need to be determined. This process parameter optimisation requires methods such as the Taguchi approach [11] or the use of process maps [12] to identify which parameters can be optimised to maximise the final density of the resulting parts. These parameters are required to aid in melt pool formation and should contribute to (1) an uninterrupted

scan track, (2) penetration and wetting of the melt pool into the previously deposited layers, and (3) deposition of material to a sufficient height to enable 3D structures [13]. The evaluation of these methods and requirements becomes very difficult for materials which are difficult to process with LPBF such as pure copper [14]. If LPBF and indeed other AM techniques are to compete successfully with traditional manufacturing techniques, automation of their various stages, including process parameter optimisation, is a necessity. AM's digital core opens an opportunity to couple it with technologies with such similar cores. One such technology is Machine Learning (ML), a subset of Artificial Intelligence (AI), that could potentially be used to improve process control and optimisation in LPBF and other AM techniques.

In AI, a program is able to accomplish a task which is typically thought to only be accomplishable by something that has some intelligence. ML furthers this concept by learning a task for which it wasn't explicitly programmed. With exposure to more data, algorithms used in ML continue to improve. Through these types of algorithms, AI has been able to perform tasks which were thought impossible a decade ago. In 2016, AI was able to make the adjustments to a 2001 Nobel prize winning experiment in under an hour [15], with these same adjustments taking a practised and experienced researcher ten times longer to determine. In 2017, AI mastered the game of chess in four hours starting from scratch [16] and mastered the game of Go without any human training in 40 days [17]. It is now able to diagnose retinal disease from 3D models at a level which matches or exceeds that of human experts [18]. Applications for AI have also prompted advances in natural language processing (Siri / Hey Google), computer vision for self-driving cars (Tesla / Waymo), and facial recognition.

There are a large number of potential applications for AI in AM. As mentioned previously, AI could be used to enhance AM process control by using images from each layer of a process such as LPBF to determine defects or problems in the build. Previous work on this sort of strategy can be seen in [19] where, a shallow ML classifier was used to identify different types of visible problems in a PBF build. AI was used as a diagnosis tool after the part was built, however, it wold be more beneficial to engage AI to monitor the build process in real-time. In [20], supervised learning was used with both images from the build and with computed tomography (CT) data after the build to detect defects which occurred during the PBF build. The learning algorithm was trained with labelled data from human subjects containing defect locations. It was found to be over 80% accurate against cross-validation data. Similarly, X-ray CT data was used in [21], where Inconel 718 was analysed using a supervised learning algorithm known as a Random Forest Network (RFN). The RFN was used to both classify defects and determine optimal processing parameters so that the researchers could narrow down the causes for different types of failure and defect in the build.

AI has also been used to assess the quality of the output from other 3D printing equipment. In [22], ML was used for droplet inspection in material jetting for the Vader Systems liquid metal jet printing machine. The network was trained to correlate an image of the output droplet with the applied voltage parameters so that the quality of the part could be monitored in real time while it was being built. In [23], AI was used to predict geometrical deviations in plastic 3D printed parts. This learned deviation of the actual printed geometry to the CAD model input can help inform the part designer of the expected tolerances of the printed part and be used to achieve higher accuracy in the end part.

To date, there seem to be little or no research published into process parameter optimization with AI techniques. A vast amount of experimental data is generated during a process parameter optimisation, much of which is represented by images of scan tracks and printed test specimens. These images could be used to correlate the quality of a part to its process parameters. Application of ML to this data could potentially reduce the high level of subjectivity currently existing in the process parameter optimisation. ML experts refer to this sort of problem as an image classification and

clustering problem, with a plethora of algorithms already developed to solve this type of challenge. Engaging these algorithms for AM techniques, could potentially accelerate process parameter optimisation, improve the quality of built parts and minimize resource wastage, thereby improving the wide appeal of AM. In this research, ML will be used with images gathered from the parameter optimisation of pure copper in order to cluster and organise the parameter sets into different levels of quality, and aid in the decision-making process to find the parameters which result in the highest quality.

Material and Methods

Powder characterisation and LPBF equipment

Pure spherically shaped copper powder was used in this work. The powder was manufactured via gas atomization using nitrogen at ECKA Granules GmbH. The process achieved an average particle size of 38.0 µm with 90% of the particles below 65.3 µm, as measured by a Mastersizer 3000 from Malvern Instruments Ltd. (UK). The powder was imaged and analysed using a desktop Hitachi TM3030 scanning electron microscope (SEM) with backscattered electron detection. The top surfaces of specimens were imaged using a Nikon Corporation Eclipse LV100ND microscope with a 2560x1920 pixel colour sensor. These images were stitched together using the built-in Nikon software. These images had all optical settings kept as constant as possible, such as brightness, white balance, contrast, and focus.

A Renishaw plc (UK) AM125 LPBF machine was used to process the copper, which was equipped with a 200-watt D Series redPOWER ytterbium fibre continuous wavelength (CW) laser from SPI Laser (UK) with a near infrared wavelength of 1070 nm (±10 nm) and a spot size of 35 µm (±5µm). This resulted in a laser power density of 20.8 MW/cm^2. The AM125 had a build volume of 125 mm^3 with a base plate heater, set to 170 °C, which was maintained throughout the build process. A vacuum and argon purge was used in the build chamber in order to keep oxygen content below a maximum of 500 parts per million, however actual processing conditions averaged below 300 ppm. Mild steel substrates were used as this has been found to be a suitable material to build copper parts upon as there is good bonding between these two materials [24].

Processing Parameters

The LPBF printing parameters in Table 1 were either varied as indicated or held constant in an investigation of the application of ML to find the optimal parameter set for maximum density.

Variable	*Value or Range*
Laser power (W)	200 (maximum available)
Laser spot diameter (µm)	35 (minimum)
Powder bed temperature (°C)	170 (maximum allowable)
Laser scan speed (mm/s)	50 to 1250 (in increments of approx. 25)
Laser point distance (µm)	30 to 200 (in increments of approx. 25)
Layer thickness (µm)	30, 45, 60
Laser beam focus position (mm)	-10 to 10 (in increments of 1, with increments of 0.2 between -1 and 1)
Hatch spacing (µm)	50 to 175 (in increments of approx. 10)

Table 1: LPBF parameters and the corresponding value or range to be tested.

Laser power, which is the optical power output of the laser beam, was used to control the amount of thermal energy transferred to the powder bed during a build. The maximum laser power was used since this is needed to re-melt previously deposited copper layers. The laser power and spot size has been and should be calibrated to ensure that the desired laser energy is supplied to the powder. It is important to note that due to high reflectivity, the full power of the laser is not absorbed into the powder,

for example, with a 1070 nm laser, copper scatters ~71% and gold scatters ~85% of incoming energy [25]. This failure to absorb all of the incoming radiant energy greatly influences the overall quality of the weld tracks. The laser usually assumes a shape similar to the frustum of a cone (Figure 2) and is characterized by a spot diameter at the point it interacts with the powder bed. The minimum spot diameter was a fixed variable within the LPBF machine (i.e. it was not adjustable by the machine users). Powder bed temperature was set to the maximum allowable value in order to pre-heat the powder and lower the energy required to melt the powder. Laser scan speed and laser point distance influence the length of time in which the laser interacts with the powder. In the Renishaw LPBF machines, the laser scan speed was calculated by the point distance divided by the laser exposure time (in μs). When a specific laser scan speed was tested, a number of point distances were also tested, and the laser exposure time was calculated and used in the Renishaw software to define the speed.

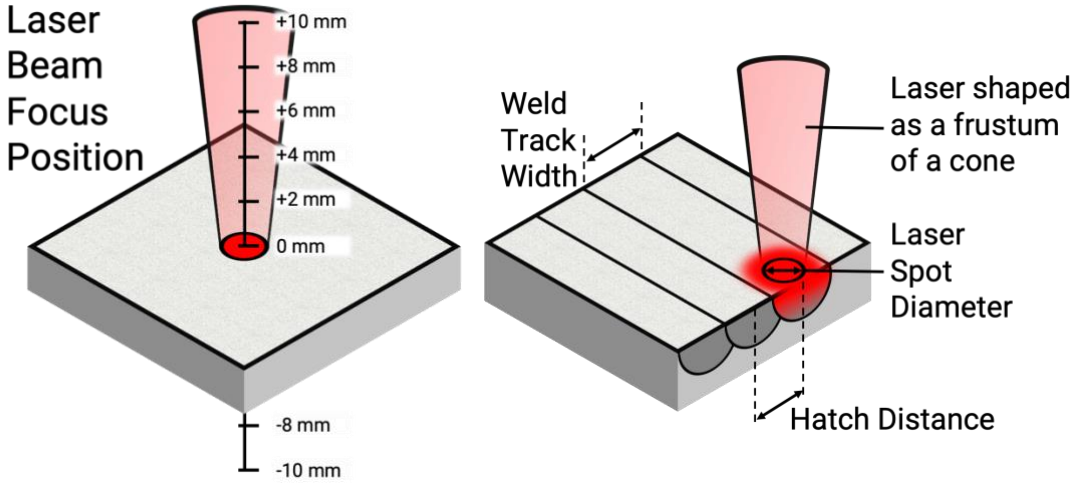

Figure 2: Example of the focus position of the laser beam (left), and example of hatch distance, laser spot diameter, and weld track width (right).

For LPBF, the layer thickness defines the amount of material that the laser needs to fully melt, and also affects how well the powder spreads on the powder bed. Thick layers spread well but make it difficult for a laser to fully melt the increased amount of material. Whereas thin layers are easier to fully melt due to having less material but may have issues spreading the powder depending on powder characteristics such as shape, size distribution, and flowability [26]. Laser beam focus position (Figure 2 left) adjusts the location of the focus and changes the energy profile of the laser spot (edges of the laser become less defined). The hatch spacing (Figure 2 right) influences the amount of overlap a laser weld track has with previous tracks in the same layer. An overlap occurs when the hatch distance is less than the weld track width and is desirable to ensure the fusion of adjacent tracks.

Multiple scans per layer attempt to increase density by melting more material than a single scan can achieve. Pre-sinter scans use laser powers less than the main scan power as a first step, in an attempt to sinter the material to aid in full melting when a second pass at full power is applied; this has been demonstrated successfully for alloys such as AlSi10Mg [27]. Remelting scan strategies attempt to melt any unmelted powders which may exist in areas of discontinuities and irregularities by using the same laser power and pattern. Similarly, the multiple scan pattern uses more than two scans per layer in addition to different laser powers per scan.

The method for parameter optimisation was as follows. First, single scan tracks were created to define the processing window for scan speed as seen in Figure 3 a). Next, thin walls were fabricated, as shown in Figure 3 b), to evaluate the intralayer bonding with

layer thickness being varied in the range 30-60 µm at intervals of 15µm. Thin walls were also used to evaluate the effect of focus position on quality. Cubes with an edge length of 5 mm were then fabricated, as seen in Figure 3 c), to evaluate hatch distance, rotation and scan strategies with respect to density and interlayer bonding. However, the results for cubes will not be reported here, as they are published separately [14].

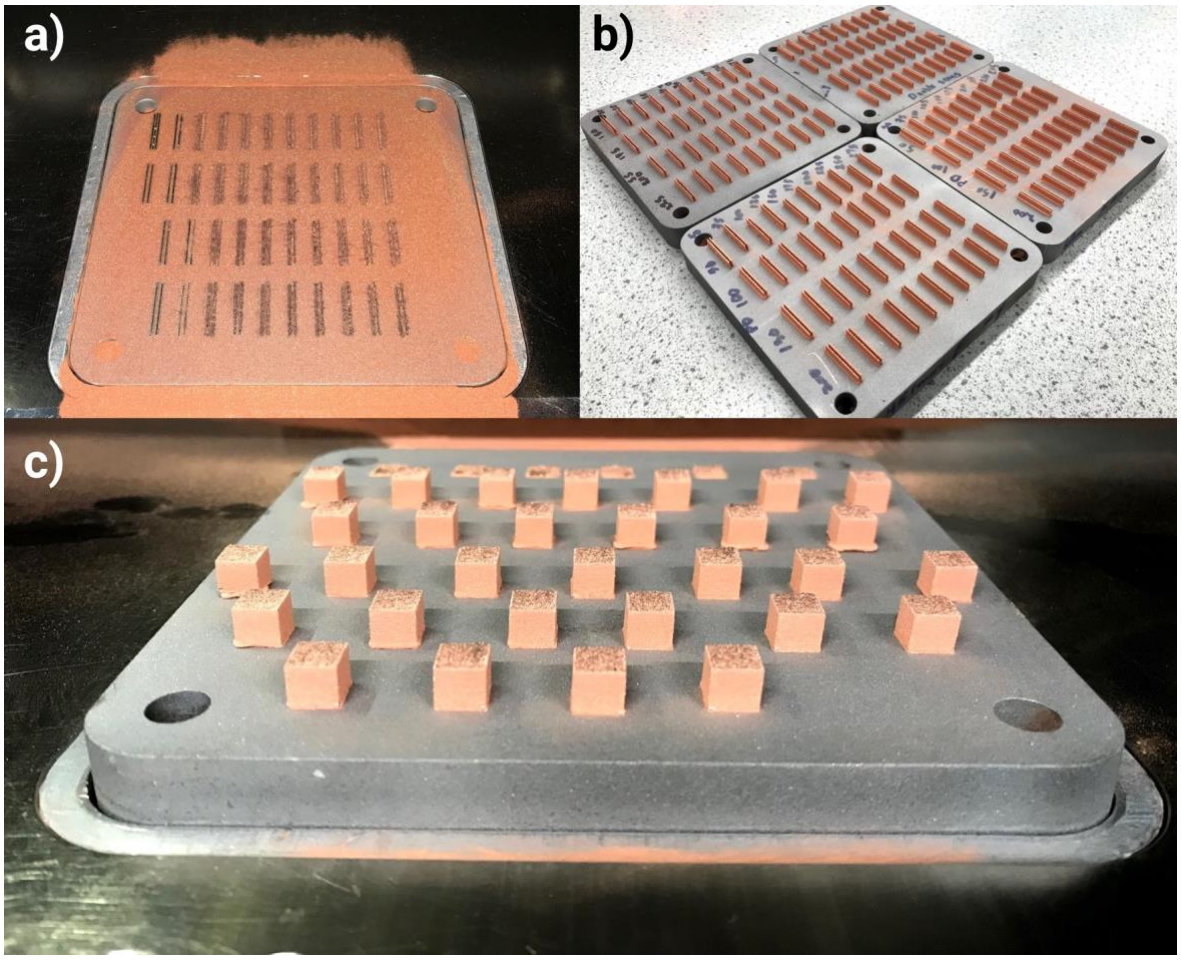

Figure 3: As-built single scan tracks a), thin walls b), and cube specimens c) of pure copper for parameter optimisation.

Software and computational methods

Machine learning

A ML algorithm was implemented with the Python 3.5 programming language [28] using Scikit-learn [29], Tensorflow [30] and Keras [31] modules. Scikit-learn was used for clustering and analytical tasks, while Tensorflow was used to implement the ML procedure for LPBF images, with Keras acting as the application programming interface (API). After images were taken of specimens on the microscope, a series of custom written macros were used to convert them into a format that would be used in ML. These macros were processed using Fiji [32] which is a version of the ImageJ software.

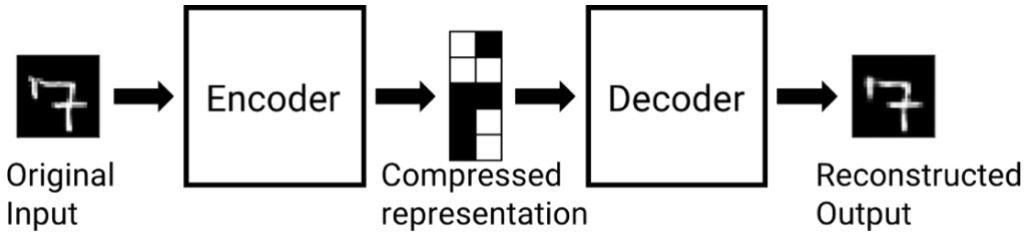

Figure 4: Typical concept for an autoencoder.

A Convolutional Neural Network (CNN) [33] was used in conjunction with an Autoencoder (AE) [34] to reduce the high-dimensional image data into a simplified reconstructed output, as seen in Figure 4. The resulting Convolutional Autoencoder (CAE) was based on the Deep Convolutional Embedded Clustering (DCEC) technique of [35], as it could be used with both labelled and non-labelled data. However, as this data was unlabelled, only the pre-training portion of the DCEC was used. In order to promote clustering, the specific architecture of [36] was used as it was found in that research that the training which occurs after the pre-training contributed less than 15-20% to the final accuracy. Thus the architecture that was used for the AE is much shallower than most, with only three convolutional layers and no flattening of the encoded latent space. The elimination of the flattening helps in feature preservation.

The autoencoder, patterned after [36], was comprised of two sets of convolutions and maximum pooling with batch normalisation, with a convolutional layer which acted as the middle latent space of the autoencoder. The remainder of the autoencoder was comprised of two sets of convolutional 2D transpose and 2D up-sampling layers along with batch normalisation. The number of convolutional filters used was 64 for the first layer, 128 for the second, and 200 for the middle latent space. The DCEC from [35], which was made opensource [37], had a number of variables which can be changed to fine-tune the process. These variables (called hyperparameters) are not learned but are pre-set before the process of learning. The hyperparameters are described in more detail in the work of [35] and [36], and include lambda set at 0.001, a batch size of 512, an alpha set to 0.9, the number of final clusters to be determined through additional analysis of the dataset, the number of nearest neighbours used being 9, and the number of top anchor points being investigated during each training being 7.

In order to determine the number of clusters which was appropriate for clustering, a method known as the gap statistic [38] was utilised. This method was designed to aid in estimation of the number of clusters within a set of data by giving a gap value for the different number of clusters, with the highest gap value indicating the optimal number of clusters. Here it was applied to the output images from the autoencoder. Initially, the latent space of the autoencoder was going to be used in clustering, however, it was found that clustering the output was more useful and informative. Before applying the gap statistic to the output images, a principle component analysis (PCA) was required on the data in order to reduce the number of dimensions, as there were 4096 dimensions for an image that was 128 x 32 pixels. PCA is a statistical method that transforms the original data to a desired number of dimensions. These new dimensions are used to explain the amount of variation that existed in the original data. The higher the number of dimensions for PCA, the better it represents the original data. However, with continuous data such as the images used in this research, lower PCA dimensions are required to find the optimal number of clusters. Too many PCA dimensions cause the gap statistic to form a logarithmic trend line which then recommends the maximum number of clusters being tested. For this data, between 2 and 10 dimensions for PCA were explored to find the optimal number of clusters, K.

The resulting ML problem is considered unsupervised, as there was no indication of what the ground truth was for these images. The ground truth is typically contained as a type

of label which is used to classify an image into a certain category. When these ground truth labels are available, the ML problem is considered supervised, as it requires supervision to create the labels. These labels could be used to identify images as either high or poor quality, or to classify the type of weld track (continuous, discontinuous, balling, etc.). Here, the ML problem is one of clustering, rather than classifying. However, if the clustering efforts accurately identify these types of labels, the data can then be labelled and used for future classification.

Results and Discussion

Traditional Parameter Optimisation

Single Scan Tracks

In determining the optimal laser scan speed, initially, the range was set to the speeds previously reported in the literature [39–42]. As laser-scan speed was defined as an exposure time and a point distance, four point distances were investigated. Pairs of tracks were used per parameter set in order to average out variations in processing. Despite the resulting tracks appearing to be of high quality, it was found that a considerable amount of iron had transported into the melt pool, as shown in Figure 5 b). While this aided in bonding to the substrate, it altered the melt characteristics and did not provide accurate information on the parameters needed for processing pure copper parts. It did however create high quality images of an ideal melt track. Thus, despite not aiding in parameter optimisation, these images were included in the data set for ML.

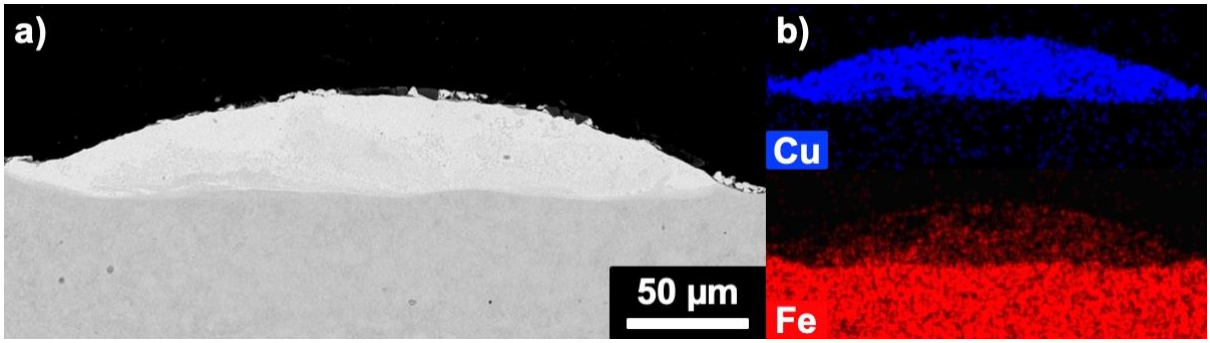

Figure 5: Cross-section of single scan track a), along with EDX analysis for copper and iron content b).

Thin Walls

The same range of laser scan speeds and point distances were used to create thin walls. This test set was repeated for the three different layer thicknesses. As with the single tracks, there was a large amount of iron diffusion into the weld tracks at slower scan speeds. An extreme example can be seen in Figure 6. In this example of a thin wall processed at 50 mm/s, iron had diffused into the melt pool from the bottom of the thin wall for approximately 1.5 mm. Once the copper concentration below the pre-melted powder layer neared 100%, the previously deposited layer with iron failed to re-melt and only pure copper was deposited. This transition from copper-iron to pure copper was characterised by a significant decrease in the wall thickness and in track quality as seen in Figure 6 b). Poor quality track images were captured for the top of these thin walls. This can be attributed to pure copper's high thermal conductivity and reflectivity to the laser wavelengths used in LPBF. These properties have made pure copper very difficult to process with LPBF and this work highlights some of these difficulties.

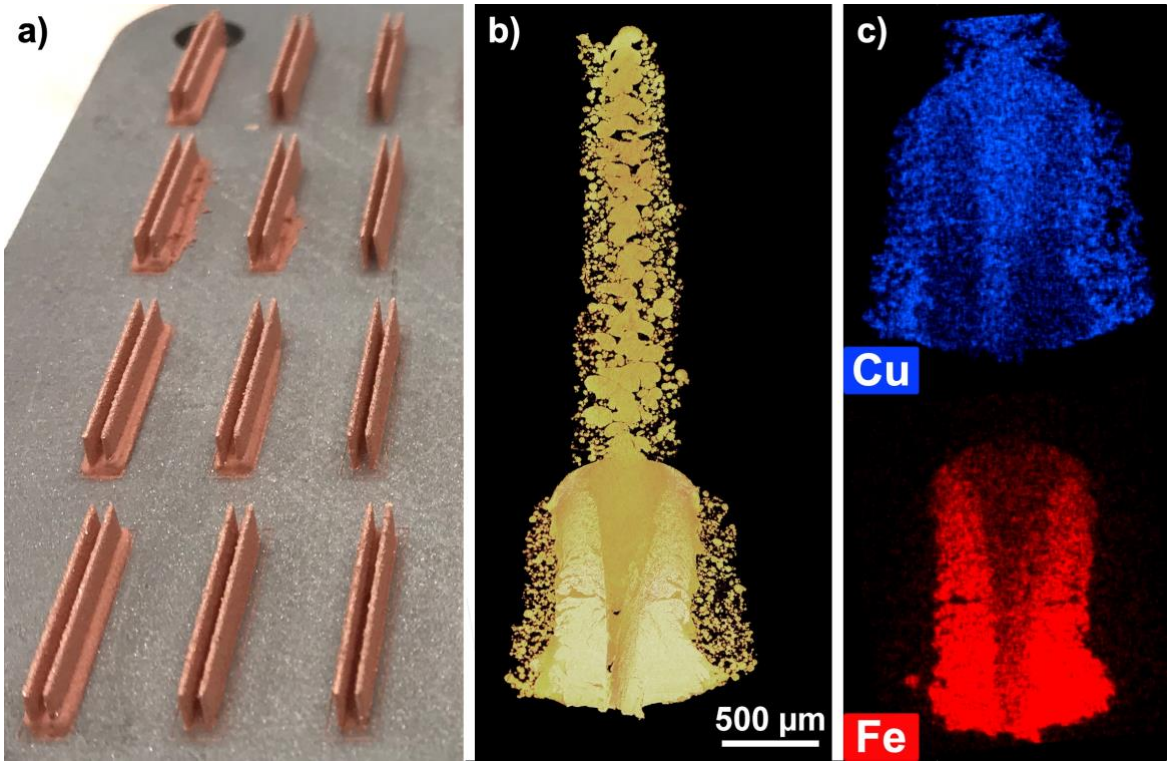

Figure 6: Thin walls in the first column on the left (a) were created at a high power and slow scan speeds, with sectioned view (b), and EDX analysis (c), that reveal copper and iron content.

When comparing the results for the three different layer thicknesses, 30 µm layers resulted in some powder spreading issues, which caused the first row of thin walls to have a raised section nearest to the powder re-coater, and random missing portions of the thin wall. The 60 µm thin walls had much less consistent weld tracks with greater amounts of sintering rather than melting. The 45 µm layers showed no signs of powder spreading issues and had much better melting behaviour than the thicker layer. For all remaining tests, a 45 µm layer thickness was used despite 30 µm being the preferred thickness due to having less material for the laser to melt.

Next, a wider range of point distances was selected to be tested at four laser speeds at maximum laser power. By comparing these tests along with the first three sets of tests used with different layer thicknesses, it was found that at many different speeds, a 50 µm point distance provided the most consistent thin wall and this was used for the remaining tests.

Finally, a wider range of laser speeds was investigated up to 1250 mm/s. It was expected that the highest laser scan speeds would not sufficiently melt the powder to form a thin wall, however, all parameters successfully resulted in thin walls. However, the fastest scan speeds did result in very thin walls with minimal bonding and low strength. After comparing the continuity of weld-tracks and thickness of the sintered particles, the best resulted from a laser scan speed of 300 mm/s produced the highest quality.

In addition to this standard optimisation, additional tests were performed as the resulting quality was still not as good as seen in the single tracks. From the previous test, the best-looking parameter set was chosen to study the effect of the laser beam focus position. Tests were conducted from -10 mm to 10 mm. Positions below -5 mm showed significant balling, and above 4 mm showed increased sintering without any improvements to weld track quality. Between -3 and 3 mm, the tracks showed similar quality with both track continuity and width of sintered particles.

The use of multiple scans for a single track were investigated as a way to try to improve the density by melting any particles that failed to form part of a continuous weld track. However, neither combinations of the different laser powers nor different orders of those laser powers failed to improve the continuity of the thin walls. Instead, multiple high-power passes only resulted in increased balling in the thin wall.

The tracks for every parameter set had the top surface imaged. An example of the range of quality visible in these images can be seen in Figure 7. After this traditional parameter optimisation was performed, it was decided that the highest quality occurred with a laser power of 200 W, layer height of 45 µm (despite preferring 30 µm layers), focus position of 0 mm, point distance of 50 µm and exposure time of 167 µs (resulting in a laser scan speed of 300 mm/s). The images from all of tested parameter sets was then used in the CAE to compare the results.

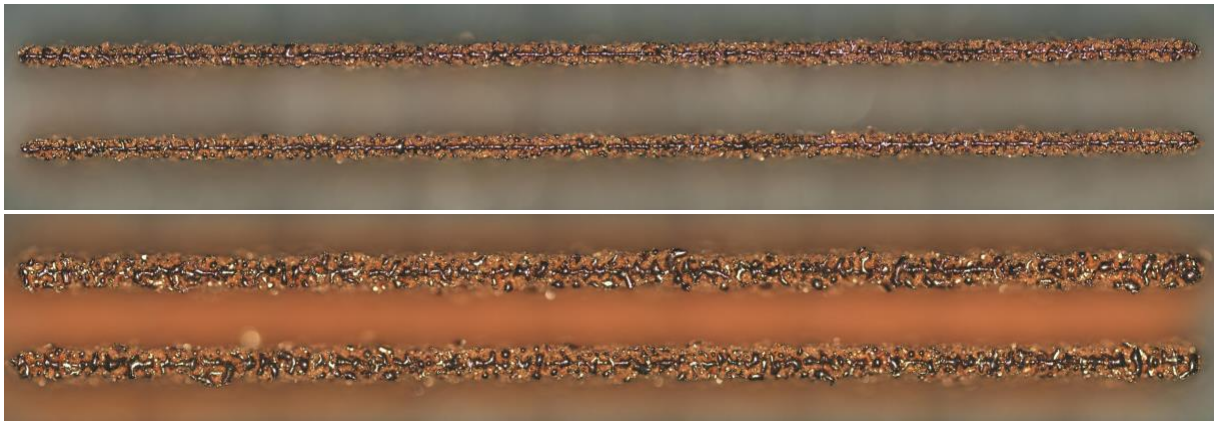

Figure 7: Pairs of 18 mm long full scan track images taken by microscope. 30 µm with a point distance of 50 µm and a scan speed of 250 mm/s (top), and 60 µm with a point distance of 200 µm and a scan speed of 75 mm/s (bottom).

Using Deep Machine Learning to measure quality

In the process of parameter optimisation, there were times when two tests appeared to have a similar quality, despite having different parameters applied. After many tests, it was possible to determine which parameter set to use, but only through the use of additional test methods such as density measurements. In order to obtain these density measurements, 5 mm cubes are manufactured using the parameters being investigated, then removed from the base plate, sectioned by a saw, mounted into resin, ground flat, polished to a mirror quality, then imaged using a microscope and manually analysed using thresholding limits in image processing software. These additional steps require a significant amount of additional time and resources. In an attempt to quicken this process and develop an alternative method for quality assessment, it was theorised that the top surface of a thin wall could be used. By imaging this top surface, and using a method to rank the corresponding quality, the time to reach the final parameters could potentially be shortened. In order to remove a human-based subjective assessment of quality, it was proposed that ML could potentially be used to learn patterns and grade the resulting thin walls.

Figure 8: Selection of random images processed and ready to feed into the autoencoder architecture.

In order to ensure that there were high quality tracks to compare within the data set, in addition to thin wall images, the single scan tracks were also included. As the autoencoder cannot take the original high-resolution 38-megapixel raw images as input (Figure 7), the images were modified. Through a series of custom-macros written for ImageJ, the images were cropped to remove the ends of the track, scaled down and de-colourised, separated into two tracks, then segmented so that the track was centred with the background removed. The final 47,448 images were grey scale (where each pixel has a value between 0 and 255) with an exact dimension of 32 pixels long by 128 pixels tall, with a random selection shown in Figure 8. After these images were run through the autoencoder, the reconstructed output removed many of the finer details that were unique to each image. This enabled the images to be better clustered to find patterns in the data. The resulting output from the autoencoder can be seen in Figure 9.

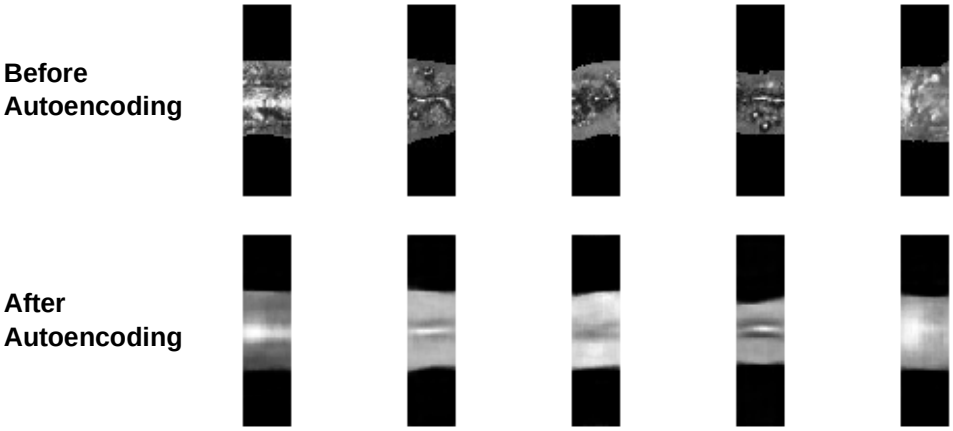

Figure 9: An example of the input images fed into the autoencoder and the resulting output image.

In order to determine the correct number of clusters to use for this data, the gap statistic was used along with principle component analysis (PCA) in order to simplify the data. For this data, between 2 and 10 dimensions for PCA were explored to find the optimal number of clusters, K, as seen Figure 10 with the highest gap value highlighted in red. Using a PCA of 2 resulted in only 2 clusters which was not large enough to correctly capture the continuous nature of the data. PCA values higher than 4 started to represent the logarithmic trend line, which was undesirable. However, a PCA value of 3 was ideal for the gap statistic to fairly determine the number of clusters to be visualised with a cluster count of 28, which was also identified with a PCA value of 4, further strengthening the idea that 28 was the ideal number of clusters.

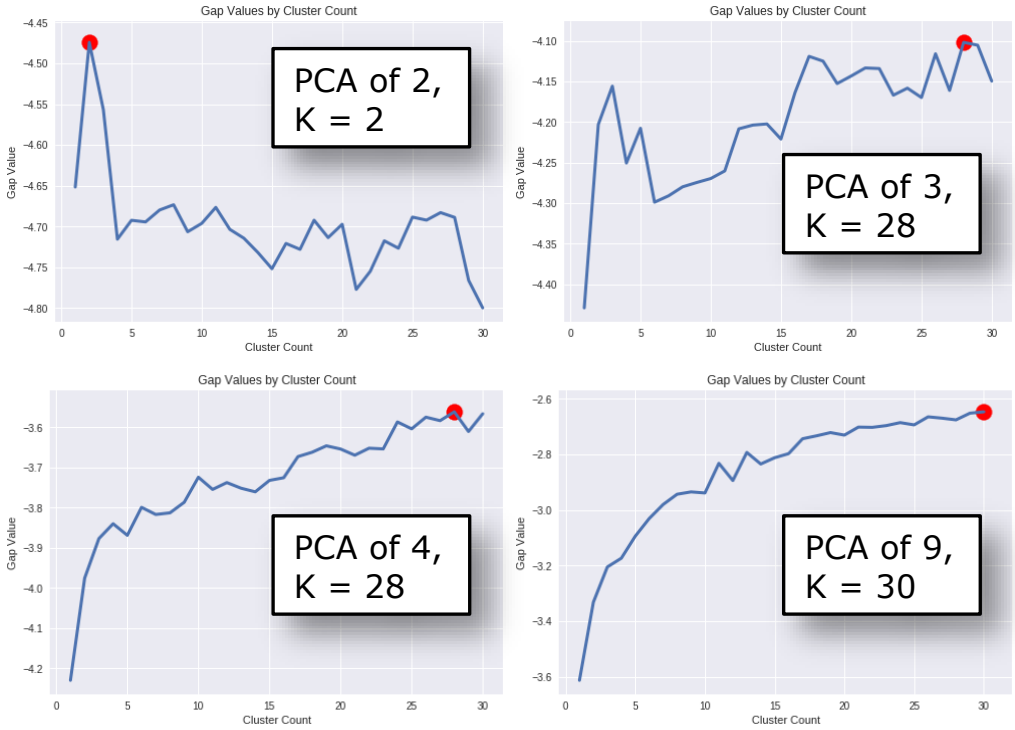

Figure 10: Gap statistic graphs indicating the ideal number of clusters in the decoded image data, with PCA value tested and resulting number of clusters.

Once the optimal number of clusters was identified, a clustering algorithm was used to classify the reduced data. Among the different clustering algorithms within Scikit-learn [29], the KMeans Mini Batch [43] algorithm was selected due to its speed and ability to report the location of cluster centres. These locations were used to obtain a number of images which were closest to them. Those images were found to be similar in appearance and fairly represented the type of image within the cluster. The clusters were then manually analysed. This was necessary because the ML was unsupervised and hence lacking the labels to separate good from bad quality weld tracks that a supervised approach would require.

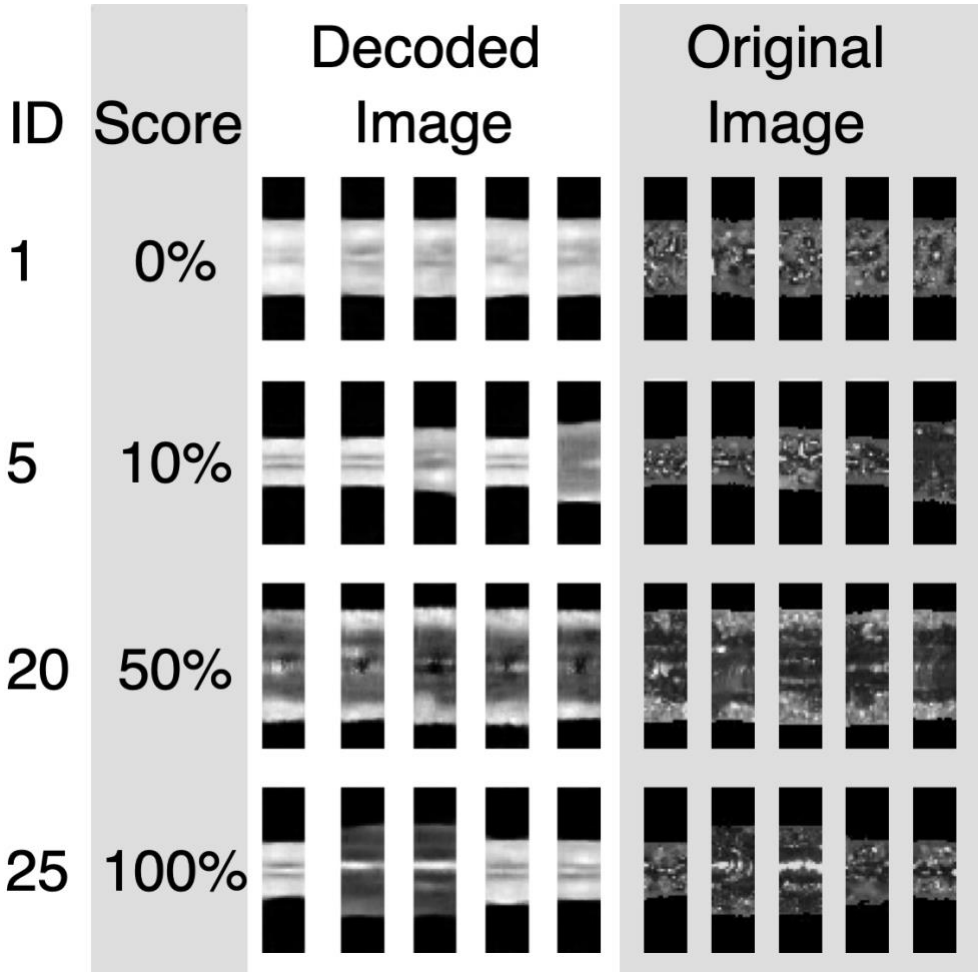

Figure 11: Sample of clustered images with a manually assigned quality score and original image.

The top 20 images from each of the 28 clusters were evaluated and scored, a selection of these are seen in Figure 11. For each cluster, a score of between 0 and 100 was applied, based on the assessed quality of the cluster. Scores of 0 were applied to clusters which showed signs of balling or an unstable melt pool. Scores of 100 were applied to clusters where the images demonstrated high quality weld tracks. For example, if all the images in a cluster showed no indication of continuous tracks, the score for the cluster was low. If some of the images in the cluster showed some well-defined continuous tracks, the cluster was scored higher. If the majority of images showed well defined and continuous tracks, it was given a maximum score of 100% despite some images appearing less than perfect. While this score did involve a human-based assessment, it was applied to a cluster of features, and not an entire track. This assessment was then applied to all tracks equally without further human-bias. Clusters had populations of between 59 and 5168 images, with sixteen clusters having a population under 1000, and nine having more than 2500 images. Each cluster contained an average of 87 unique parameter sets within the cluster. As the images still retained the original parameter set which created it, the scores for the clusters were then applied to the entire scan track, giving a total score for the set of parameters which went into the creation of the tracks. Based on the scores, results were compared with observations from the traditional parameter optimisation process discussed earlier.

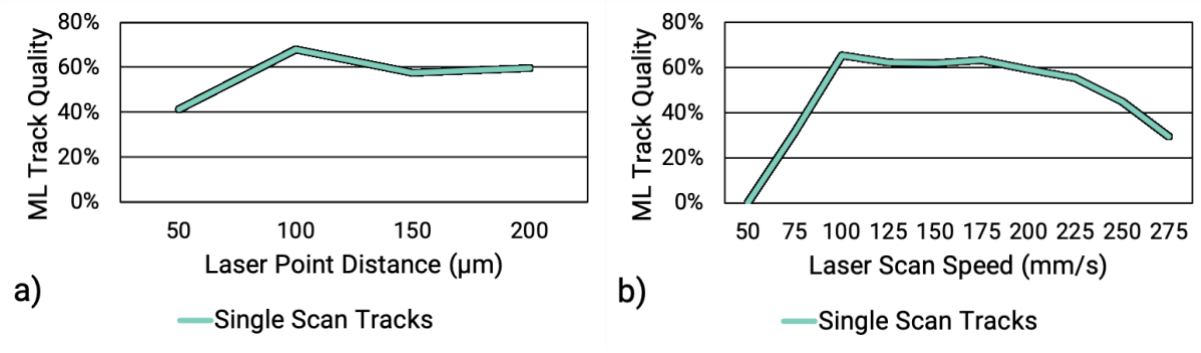

Figure 12: Single scan track ML quality verses laser point distance a), and laser scan speed b).

The first insight from analysis of the results of the ML exercise is in the quality of single tracks compared to thin walls. The average score for single tracks was 68%, compared to 3% for thin walls. This agrees with the results found from the microscopic study discussed previously, which demonstrated that for the single tracks iron transported into the melt pool created perfect looking weld tracks. These iron-infused weld tracks were well defined and showed very little signs of balling. In comparing the laser point distance for single tracks in Figure 12, there was not much score variation, with 50 µm being the lowest despite it being chosen as the best point distance. In comparing laser scan speeds however, speeds below 100 mm/s scored poorly as those tracks had excess laser power and lacked any copper tracks in the images.

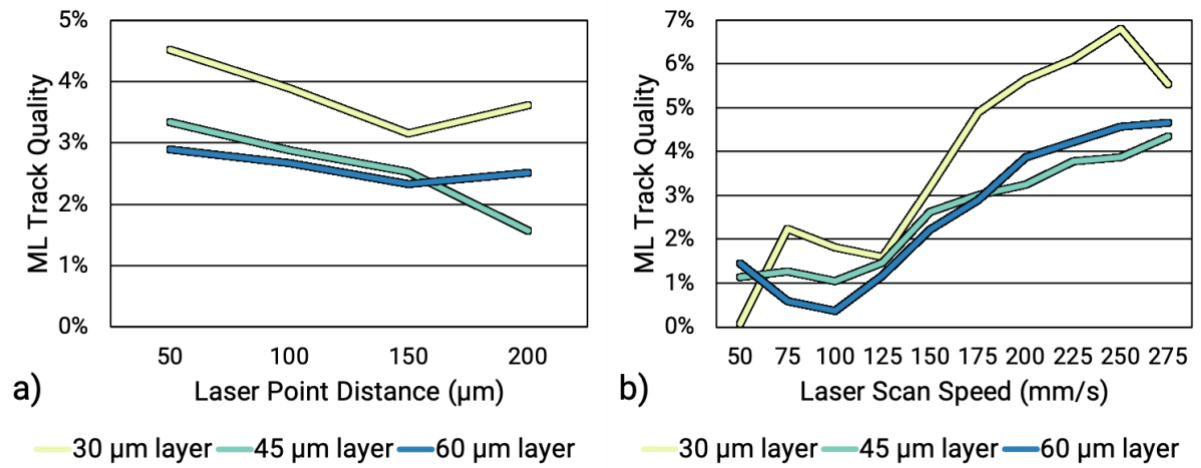

Figure 13: Thin wall ML track quality verses laser point distance a), and scan speed b) at different layer thicknesses.

The machine learned scores for different layer thicknesses with regards to the laser scan speed and point distance showed similar trends to the traditional parameter optimisation process. In Figure 13, the scores show that for all layer thicknesses, a 50 µm point distance and laser scan speeds of 250 mm/s and above created the best tracks. This confirmed that if there were no powder spreading issues associated with the 30 µm layer, it would have produced better looking and higher quality tracks verses the 45 µm layer.

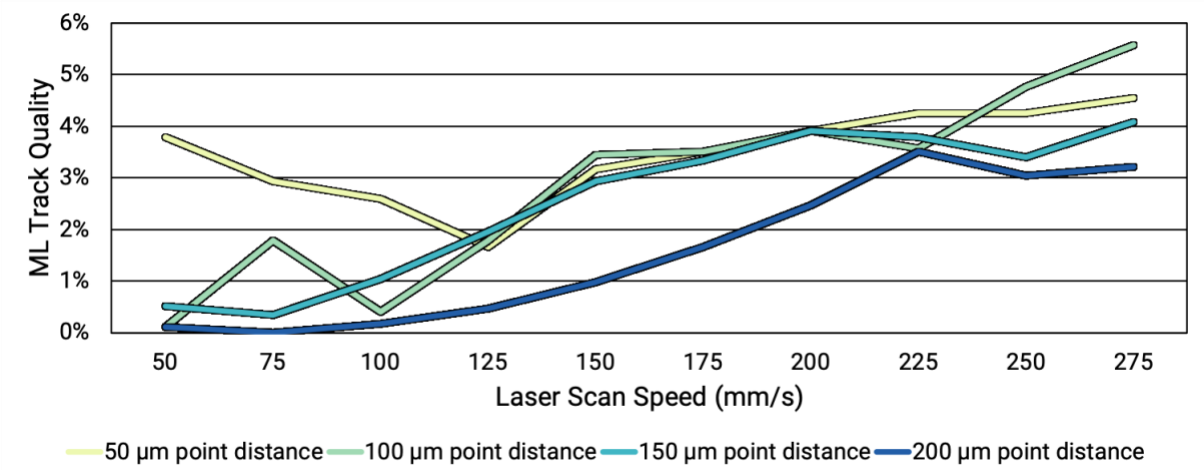

Figure 14: ML track quality for different laser scan speeds and at different laser point distances.

In the traditional parameter optimisation process, once the 45 µm layer thickness was chosen, additional thin walls were created in order to determine the best laser scan speed and laser point distance, as it was not as clear from the visual examination of the tracks that 50 µm was the best point distance. Again, as seen in Figure 14, the ML score results showed that 50 µm was still the best laser point distance with speeds of 275 mm/s (or greater) which resulted in the best quality tracks. However, in examining the ML results which explored point distances from 20 to 175 µm at speeds of 150 to 225 mm/s, there was no discernable difference in ML track quality scores, as all quality scores fell between 3-6% with no visible trend for either point distance or laser scan speed. This differed from visual examination which indicated that 50 µm was the best laser point distance.

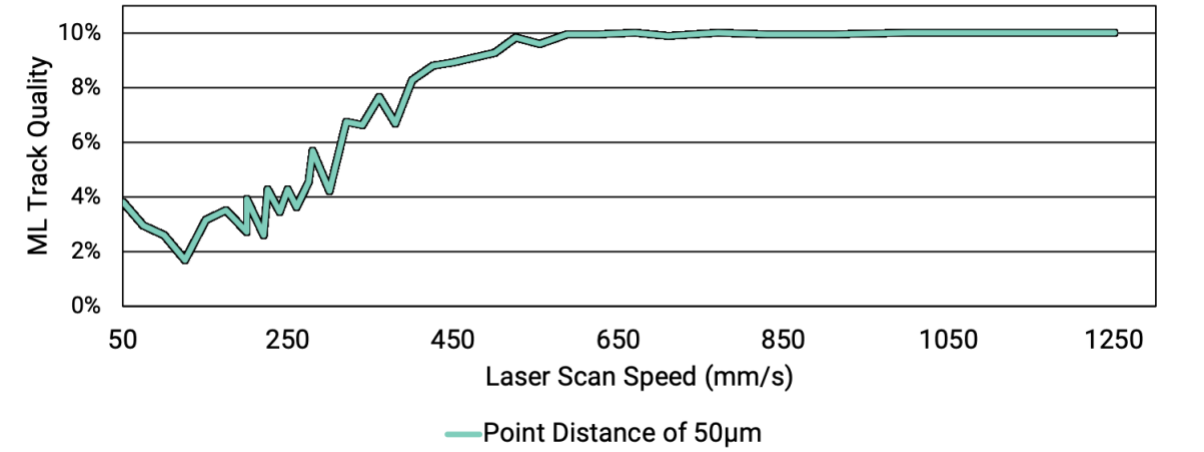

Figure 15: ML track quality for different laser scan speeds with the same 50 µm point distance.

In order to determine the best speed, the next test for parameter optimization was to increase the range of laser scan speeds up to 1250 mm/s, with ML scores seen in Figure 15. These high speeds were intended to go beyond the point that a track would no longer form, however, all speeds resulted in the creation of a track, although with the highest speeds creating very thin and weak walls. In terms of laser scan speed, the results from ML differed from the traditional parameter optimisation, the latter indicating that speeds of 300 mm/s resulted in the best quality, whereas ML indicated that speeds above 500 mm/s resulted in tracks of the highest quality. This was wrongly implied due to the scoring assignment used. There were many clusters which were given scores of 10

due to having some fine thin weld tracks, which were desirable, along with examples of discontinuous tracks within the cluster. As high speeds tended to result in consistent looking thin walls, they happened to also correspond to one of the resulting clusters which was scored as a 10. That was why speeds above 500 mm/s plateaued at 10%.

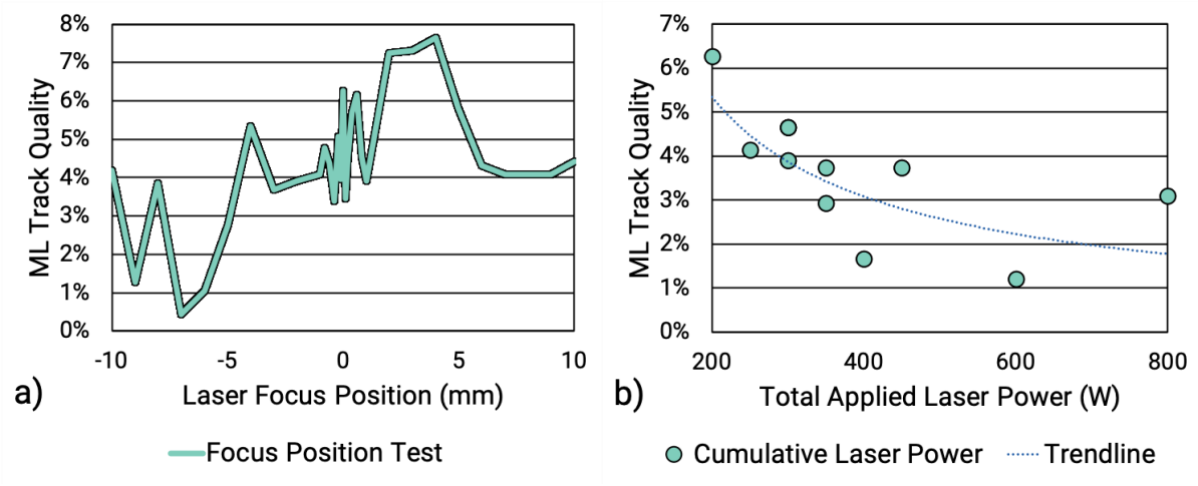

Figure 16: ML track quality for laser focus tests a), and total wattage applied for multiple laser passes b).

In Figure 16 a), the laser focus position test scores showed that the zero-position was just over 6%, with only the positions of two to four being higher at just over 7%. This closely matched the actual results which found that the positions between -3 to 3 were similar in quality. But this result could indicate that perhaps more tests should be performed to confirm if those higher scores are reliable. In Figure 16 b), the scores were graphed against the total wattage applied by multiple passes of the laser. For example, the point above 200 was a single pass at 200 W, whereas 600 was generated by three passes at 200 W. These scores match the optimisation results as all multiple passes were found to be lower quality with high amounts of balling.

Overall, the results of this clustering and scoring method has shown that ML can aid in the typical parameter optimisation process. While disparities exist between ML and traditional optimization process, such as the convergence of scores at higher speeds, generally the trends followed the same results. This is a consequence of limited diversity in the data used in the image classification which lacked information about parameter sets needed for high quality thin walls. There is still an opportunity to improve the scoring procedure and also to add more data in conjunction to image data such as laser energy density into parameter optimisation and potentially move this highly manual step into more of an automated process via ML.

Conclusions

Machine learning was used in an attempt to see if it could aid in the parameter optimisation process. Parameter optimisation is currently a manual process which relies on human judgement to determine whether one set of parameters is better than another. But by using machine learning, an alternative method to determine this optimal set can be derived. Data in the form of optical images was collected over the course of a traditional parameter optimisation. These large images were segmented and fed into a convolutional autoencoder and then clustered in order to find the clusters which best represented a high-quality result. The clusters were manually scored according to quality and the results were applied to the original sets of parameters. It was found that the machine learned clustering and subsequent scoring reflected many of the observations which were found in the traditional parameter optimisation process, and did match the trends for deciding the optimal laser point distance, powder layer thickness, and laser

scanning speed. While it is not a perfect predictor, with more data this approach could be made more robust and automated. Machine learning opens up an opportunity to automate some steps of parameter optimisation in order to conform more alloys to the laser powder bed fusion technique.

The potential for machine learning is limited by the availability of data. As the only data used for this was gathered from a single parameter optimisation study for a single material, which wasn't able to be processed to a high density, there is a lot of room for improvement to create a more robust algorithm. By incorporating additional parameter optimisation studies with additional materials, the process could be made more accurate. There is also a potential to then apply labels to the clusters of data, so that the process could become more automated as the algorithm would be able to assess the quality of a cluster on-the-fly. This latter ability could then potentially be further developed to enable in-process parameter control and optimisation.

Acknowledgements

This research did not receive any specific grant from funding agencies in the public, commercial, or not-for-profit sectors.

References

[1] N. Hopkinson, R. Hague, P.M. Dickens, Rapid Manufacturing, John Wiley & Sons, Ltd, Chichester, UK, 2005. doi:10.1002/0470033991.

[2] G.N. Levy, R. Schindel, Overview of layer manufacturing technologies, opportunities, options and applications for rapid tooling, Proc. Inst. Mech. Eng. Part B J. Eng. Manuf. 216 (2002) 1621–1634. doi:10.1243/095440502321016350.

[3] J.J. Beaman, J.W. Barlow, D.L. Bourell, R.H. Crawford, H.L. Marcus, K.P. McAlea, Solid Freeform Fabrication: A New Direction in Manufacturing, Springer US, Boston, Massachusetts, USA, 1997. doi:10.1007/978-1-4615-6327-3.

[4] J.-P. Kruth, M.C. Leu, T. Nakagawa, Progress in additive manufacturing and rapid prototyping, CIRP Ann. - Manuf. Technol. 47 (1998) 525–540. doi:10.1016/s0007-8506(07)63240-5.

[5] ASTM ISO/ASTM52900-15 Standard Terminology for Additive Manufacturing – General Principles – Terminology, ASTM International, West Conshohocken, Pennsylvania, USA, 2015. doi:10.1520/isoastm52900-15.

[6] N. Buchanan, An example of Laser Powder Bed Fusion (LPBF), (2018). https://redheaddirection.com/.

[7] I. Gibson, A. Srinath, Simplifying medical additive manufacturing: Making the surgeon the designer, Procedia Technol. 20 (2015) 237–242.

[8] S.L. Sing, J. An, W.Y. Yeong, F.E. Wiria, Laser and electron-beam powder-bed additive manufacturing of metallic implants: A review on processes, materials and designs, J. Orthop. Res. 34 (2016) 369–385. doi:10.1002/jor.23075.

[9] R. Leal, F.M. Barreiros, L. Alves, F. Romeiro, J.C. Vasco, M. Santos, C. Marto, Additive manufacturing tooling for the automotive industry, Int. J. Adv. Manuf. Technol. 92 (2017) 1671–1676. doi:10.1007/s00170-017-0239-8.

[10] B.P. Conner, G.P. Manogharan, A.N. Martof, L.M. Rodomsky, C.M. Rodomsky, D.C. Jordan, J.W. Limperos, Making sense of 3-D printing: Creating a map of additive manufacturing products and services, Addit. Manuf. 1–4 (2014) 64–76. doi:10.1016/j.addma.2014.08.005.

[11] J. Sun, Y. Yang, D. Wang, Parametric optimization of selective laser melting for forming Ti6Al4V samples by Taguchi method, Opt. Laser Technol. 49 (2013) 118–124. doi:10.1016/j.optlastec.2012.12.002.

[12] J. Beuth, N. Klingbeil, The role of process variables in laser-based direct metal solid freeform fabrication, Jom. 53 (2001) 36–39. doi:10.1007/s11837-001-0067-y.

[13] K. Kempen, L. Thijs, J. Van Humbeeck, J.-P. Kruth, Processing AlSi10Mg by selective laser melting: parameter optimisation and material characterisation, Mater. Sci. Technol. 31 (2015) 917–923. doi:10.1179/1743284714Y.0000000702.

[14] C. Silbernagel, L. Gargalis, I. Ashcroft, R. Hague, M. Galea, P. Dickens, Electrical resistivity of pure copper processed by medium-powered laser powder bed fusion additive manufacturing for use in electromagnetic applications, Addit. Manuf. 29 (2019) 100831. doi:10.1016/j.addma.2019.100831.

[15] P.B. Wigley, P.J. Everitt, A. van den Hengel, J.W. Bastian, M.A. Sooriyabandara, G.D. McDonald, K.S. Hardman, C.D. Quinlivan, P. Manju, C.C.N. Kuhn, I.R. Petersen, A.N. Luiten, J.J. Hope, N.P. Robins, M.R. Hush, Fast machine-learning online optimization of ultra-cold-atom experiments, Sci. Rep. 6 (2016) 25890. doi:10.1038/srep25890.

[16] D. Silver, T. Hubert, J. Schrittwieser, I. Antonoglou, M. Lai, A. Guez, M. Lanctot, L. Sifre, D. Kumaran, T. Graepel, T. Lillicrap, K. Simonyan, D. Hassabis, Mastering chess and shogi by self-play with a general reinforcement learning algorithm, (2017). http://arxiv.org/abs/1712.01815.

[17] D. Silver, J. Schrittwieser, K. Simonyan, I. Antonoglou, A. Huang, A. Guez, T. Hubert, L. Baker, M. Lai, A. Bolton, Y. Chen, T. Lillicrap, F. Hui, L. Sifre, G. van den Driessche, T. Graepel, D. Hassabis, Mastering the game of Go without human knowledge, Nature. 550 (2017) 354–359. doi:10.1038/nature24270.

[18] J. De Fauw, J.R. Ledsam, B. Romera-Paredes, S. Nikolov, N. Tomasev, S. Blackwell, H. Askham, X. Glorot, B. O'Donoghue, D. Visentin, G. van den Driessche, B. Lakshminarayanan, C. Meyer, F. Mackinder, S. Bouton, K. Ayoub, R. Chopra, D. King, A. Karthikesalingam, C.O. Hughes, R. Raine, J. Hughes, D.A. Sim, C. Egan, A. Tufail, H. Montgomery, D. Hassabis, G. Rees, T. Back, P.T. Khaw, M. Suleyman, J. Cornebise, P.A. Keane, O. Ronneberger, Clinically applicable deep learning for diagnosis and referral in retinal disease, Nat. Med. 24 (2018) 1342–1350. doi:10.1038/s41591-018-0107-6.

[19] L. Scime, J. Beuth, Anomaly detection and classification in a laser powder bed additive manufacturing process using a trained computer vision algorithm, Addit. Manuf. 19 (2018) 114–126. doi:10.1016/j.addma.2017.11.009.

[20] C. Gobert, E.W. Reutzel, J. Petrich, A.R. Nassar, S. Phoha, Application of supervised machine learning for defect detection during metallic powder bed fusion additive manufacturing using high resolution imaging., Addit. Manuf. 21 (2018) 517–528. doi:10.1016/j.addma.2018.04.005.

[21] B. Kappes, S. Moorthy, D. Drake, H. Geerlings, A. Stebner, Machine learning to optimize additive manufacturing parameters for laser powder bed fusion of Inconel 718, in: Proc. 9th Int. Symp. Superalloy 718 Deriv. Energy, Aerospace, Ind. Appl., Springer International Publishing, Pittsburgh, Pennsylvania, USA, 2018: pp. 595–610. doi:10.1007/978-3-319-89480-5_39.

[22] T. Wang, T.-H. Kwok, C. Zhou, S. Vader, In-situ droplet inspection and closed-loop control system using machine learning for liquid metal jet printing, J. Manuf. Syst. 47 (2018) 83–92. doi:10.1016/j.jmsy.2018.04.003.

[23] Z. Zhu, N. Anwer, Q. Huang, L. Mathieu, Machine learning in tolerancing for additive manufacturing, CIRP Ann. 67 (2018) 157–160. doi:10.1016/j.cirp.2018.04.119.

[24] S.R.R. Pogson, P. Fox, C.J.J. Sutcliffe, W. O'Neill, The production of copper parts using DMLR, Rapid Prototyp. J. 9 (2003) 334–343. doi:10.1108/13552540310502239.

[25] M. Khan, Selective laser melting (SLM) of gold (Au), Loughborough University, 2010. https://dspace.lboro.ac.uk/2134/6163.

[26] A.B. Spierings, G. Levy, Comparison of Density of Stainless Steel 316L Parts Produced With Selective Laser Melting Using Different Powder Grades, in: Proc. 20th Solid Free. Fabr. Symp., Austin, Texas, USA, 2009: pp. 342–353. http://sffsymposium.engr.utexas.edu/Manuscripts/2009/2009-30-Spierings.pdf.

[27] N.T. Aboulkhair, N.M. Everitt, I. Ashcroft, C. Tuck, Reducing porosity in AlSi10Mg parts processed by selective laser melting, Addit. Manuf. 1–4 (2014) 77–86. doi:10.1016/j.addma.2014.08.001.

[28] G. Van Rossum, F.L. Drake Jr, Python reference manual, Centrum voor Wiskunde en Informatica Amsterdam, Amsterdam, The Netherlands, The Netherlands, 1995. https://docs.python.org/3/.

[29] F. Pedregosa, G. Varoquaux, A. Gramfort, V. Michel, B. Thirion, O. Grisel, M. Blondel, P. Prettenhofer, R. Weiss, V. Dubourg, Scikit-learn: Machine learning in Python, J. Mach. Learn. Res. 12 (2011) 2825–2830. https://dl.acm.org/citation.cfm?id=2078195.

[30] M. Abadi, A. Agarwal, P. Barham, E. Brevdo, Z. Chen, C. Citro, G.S. Corrado, A. Davis, J. Dean, M. Devin, S. Ghemawat, I. Goodfellow, A. Harp, G. Irving, M. Isard, R. Jozefowicz, Y. Jia, L. Kaiser, M. Kudlur, J. Levenberg, D. Mané, M. Schuster, R. Monga, S. Moore, D. Murray, C. Olah, J. Shlens, B. Steiner, I. Sutskever, K. Talwar, P. Tucker, V. Vanhoucke, V. Vasudevan, F. Viégas, O. Vinyals, P. Warden, M. Wattenberg, M. Wicke, Y. Yu, X. Zheng, TensorFlow: Large-scale machine learning on heterogeneous systems, (2015). https://www.tensorflow.org/.

[31] F. Chollet, Keras, (2015). https://keras.io.

[32] J. Schindelin, I. Arganda-Carreras, E. Frise, V. Kaynig, M. Longair, T. Pietzsch, S. Preibisch, C. Rueden, S. Saalfeld, B. Schmid, J.-Y. Tinevez, D.J. White, V. Hartenstein, K. Eliceiri, P. Tomancak, A. Cardona, Fiji: An open-source platform for biological-image analysis, Nat. Methods. 9 (2012) 676–682. doi:10.1038/nmeth.2019.

[33] Y. Lecun, L. Bottou, Y. Bengio, P. Haffner, Gradient-based learning applied to document recognition, Proc. IEEE. 86 (1998) 2278–2324. doi:10.1109/5.726791.

[34] G.E. Hinton, R.R. Salakhutdinov, Reducing the dimensionality of data with neural networks, Science (80-.). 313 (2006) 504–507. doi:10.1126/science.1127647.

[35] X. Guo, X. Liu, E. Zhu, J. Yin, Deep clustering with convolutional autoencoders, in: Lect. Notes Comput. Sci. (Including Subser. Lect. Notes Artif. Intell. Lect. Notes Bioinformatics), 2017: pp. 373–382. doi:10.1007/978-3-319-70096-0_39.

[36] E. Tzoreff, O. Kogan, Y. Choukroun, Deep discriminative latent space for clustering, ArXiv Prepr. 1805.10795. (2018). https://arxiv.org/abs/1805.10795v1.

[37] X. Guo, XifengGuo/DCEC, (2017). https://github.com/xifengguo/dcec (accessed June 22, 2018).

[38] R. Tibshirani, G. Walther, T. Hastie, Estimating the number of clusters in a data set via the gap statistic, J. R. Stat. Soc. Ser. B (Statistical Methodol. 63 (2001) 411–423. doi:10.1111/1467-9868.00293.

[39] J.B. Jones, D.I. Wimpenny, R. Chudasama, G.J. Gibbons, Printed circuit boards by selective deposition and processing, in: Proc. 22nd Solid Free. Fabr. Symp., Austin, Texas, USA, 2011: pp. 639–656. http://sffsymposium.engr.utexas.edu/Manuscripts/2011/2011-50-Jones.pdf.

[40] P.A. Lykov, E.V. Safonov, A.M. Akhmedianov, Selective laser melting of copper, Mater. Sci. Forum. 843 (2016) 284–288. doi:10.4028/www.scientific.net/msf.843.284.

[41] T. El-Wardany, Y. She, V. Jagdale, J.K. Garofano, J. Liou, W. Schmidt, Challenges in 3D printing of high conductivity copper, in: ASME 2017 Int. Tech. Conf. Exhib. Packag. Integr. Electron. Photonic Microsystems, ASME, San Francisco, California, USA, 2017. doi:10.1115/ipack2017-74306.

[42] T.-T.T.T. Ikeshoji, K. Nakamura, M. Yonehara, K. Imai, H. Kyogoku, Selective laser melting of copper, JOM. (2017) 3–7. doi:10.1007/s11837-017-2695-x.

[43] D. Sculley, Web-scale k-means clustering, in: Proc. 19th Int. World Wide Web Conf. (WWW '10), ACM Press, Raleigh, North Carolina, USA, 2010: pp. 1177–1178. doi:10.1145/1772690.1772862.